Temperature Dependence of Electron Transfer to the M-Side Bacteriopheophytin in *Rhodobacter capsulatus* Reaction Centers

Jessica I. Chuang,[†,#] Steven G. Boxer,[†] Dewey Holten,[‡] and Christine Kirmaier*[,‡]

Department of Chemistry, Stanford University, Stanford, California 94305-5080, and Department of Chemistry, Washington University, St. Louis, Missouri 63130-4899

Received: January 4, 2008; In Final Form: February 8, 2008

Subpicosecond time-resolved absorption measurements at 77 K on two reaction center (RC) mutants of *Rhodobacter capsulatus* are reported. In the D_{LL} mutant the D helix of the M subunit has been substituted with the D helix from the L subunit, and in the D_{LL}-FY_LF_M mutant, three additional mutations are incorporated that facilitate electron transfer to the M side of the RC. In both cases the helix swap has been shown to yield isolated RCs that are devoid of the native bacteriopheophytin electron carrier H_L (Chuang, J. I.; Boxer, S. G.; Holten, D.; Kirmaier, C. *Biochemistry* **2006**, *45*, 3845−3851). For D_{LL}, depending whether the detergent Deriphat 160-C or *N*-lauryl-*N*,*N*-dimethylamine-*N*-oxide (LDAO) is used to suspend the RCs, the excited state of the primary electron donor (P*) decays to the ground state with an average lifetime at 77 K of 330 or 170 ps, respectively; however, in both cases the time constant obtained from single-exponential fits varies markedly as a function of the probe wavelength. These findings on the D_{LL} RC are most easily explained in terms of a heterogeneous population of RCs. Similarly, the complex results for D_{LL}-FY_LF_M in Deriphat−glycerol glass at 77 K are most simply explained using a model that involves (minimally) two distinct populations of RCs with very different photochemistry. Within this framework, in 50% of the D_{LL}-FY_LF_M RCs in Deriphat−glycerol glass at 77 K, P* deactivates to the ground state with a time constant of ∼400 ps, similar to the deactivation of P* in the D_{LL} mutant at 77 K. In the other 50% of D_{LL}-FY_LF_M RCs, P* has a 35 ps lifetime and decays via electron transfer to the M branch, giving $P^+H_M^-$ in high yield (≥80%). This result indicates that $P^* \rightarrow P^+H_M^-$ is roughly a factor of 2 *faster* at 77 K than at 295 K. In alternative homogeneous models the rate of this M-side electron-transfer process is the same or up to 2-fold slower at low temperature. A 2-fold increase in rate with a reduction in temperature is the same behavior found for the overall L-side process $P^* \rightarrow P^+H_L^-$ in wild-type RCs. Our results suggest that, as for electron transfer on the L side, the M-side electron-transfer reaction $P^* \rightarrow P^+H_M^-$ is an activationless process.

Introduction

Bacterial photosynthetic reaction centers (RCs) perform highly efficient, unidirectional electron transfer. For each photon absorbed by the primary electron donor pair (P), a dimer of bacteriochlorophyll (BChl) molecules, an electron is transferred via the cofactors on the so-called L branch (also referred to as the A branch) to quinone Q_A, as indicated with the arrows in Figure 1A. Subsequent electron transfer then occurs to the final acceptor Q_B. The presence of two possible electron-transfer pathways related by a local C_2 axis of symmetry is evident in the RC structure, but the pathway symmetry is broken by differences in amino acids around the cofactors.[1−6] These differences inhibit charge separation to the cofactors on the M branch (also referred to as the B branch) in the wild-type RC, while facilitating electron transfer to the L-side bacteriopheophytin (H_L) in ∼2.8 ps in *Bastochloris viridis* and *Rhodobacter (Rb.) sphaeroides* and ∼4.2 ps in *Rb. capsulatus* RCs.[7−10] At cryogenic temperatures (77 K and lower) the reduction of H_L is even faster, ∼0.7, ∼1.2, ∼2.0 ps, in RCs from these same three species, respectively.[7,10−14] Subsequent $P^+H_L^- \rightarrow P^+Q_A^-$ electron transfer exhibits a similar temperature dependence with the time constant decreasing from ∼200 ps at room temperature to ∼100 ps at low temperature.[10,15]

Although a given RC sample (wild type or mutant) is commonly evaluated as a homogeneous population, many experiments have suggested otherwise. A variety of results have been discussed in terms of heterogeneous populations of RCs composed of a distribution of forms, and in some cases these data have been analyzed most simply in terms of two forms of RCs. Evidence for this heterogeneity has come from a variety of measurements exploring parameters such as buffer or detergent properties, pH, or temperature. RC properties found to be affected include the position of the long-wavelength absorption band of P, the electronic structure of P^+, the P/P^+ midpoint potential, the P* lifetime, the rate of $P^+H_L^- \rightarrow P^+Q_A^-$ electron transfer, and the rate of $P^+Q_A^- \rightarrow$ ground state charge recombination.[14,16−49] For example, although a single value for the P* lifetime is often quoted for wild-type and mutant RCs the decay kinetics are more complex and no obvious correlations have been found between mutational perturbations made in the RC and the range or temperature dependence of the observed time constants.

Unidirectional electron transfer in wild-type RCs is thought to be governed by differences between the free energies of the

* To whom correspondence should be addressed. Phone: 314-935-6480. Fax: 314-935-4481. E-mail: kirmaier@wustl.edu.
† Stanford University.
‡ Washington University.
# Current address: University of California, Department of Chemistry, Berkeley, CA 94720-1460.

10.1021/jp800082m CCC: $40.75
Published on Web 04/11/2008

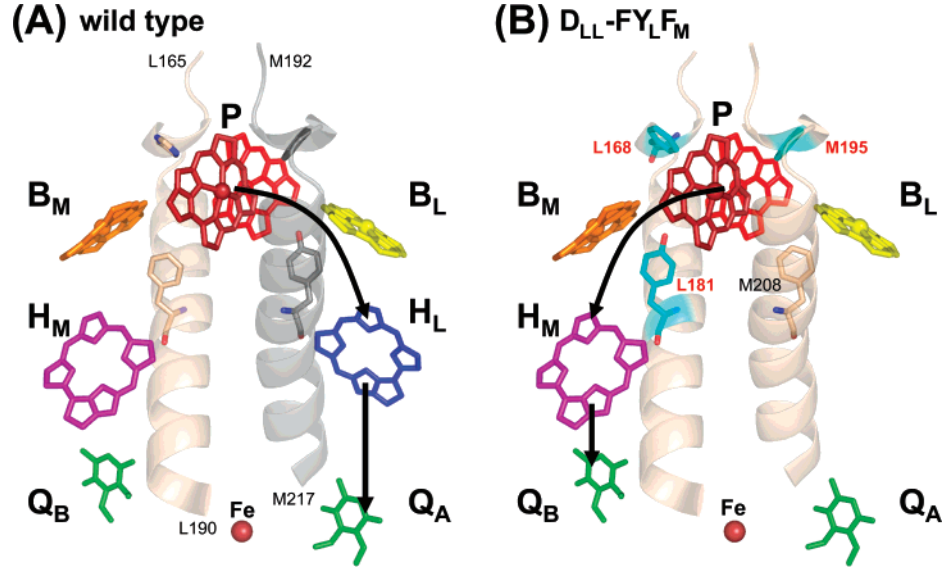

Figure 1. (A) Arrangement of the wild-type L- and M-branch cofactors and the portion of the L polypeptide D helix (left helix) that is duplicated as the M polypeptide D helix (right helix) in D_{LL}. Key C_2 symmetry-related amino acid pairs, His−L168 and Phe−M195, and Phe−L181 and Tyr−M208, are located as shown. (B) In D_{LL} H_L is missing and M208 is changed to Phe as a result of the helix swap. Additionally, in the mutant D_{LL}-FY_LF_M residues L168 and M195 were mutated to Phe and L181 to Tyr.

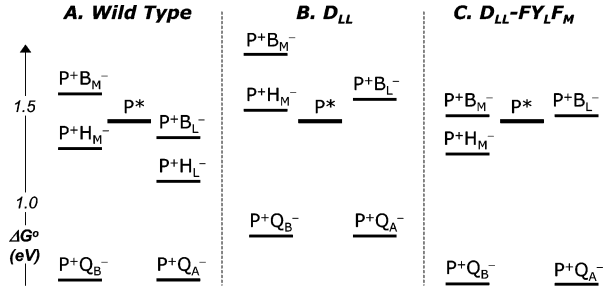

Figure 2. Working models proposed for the relative free energies of the charge-separated states in RCs from (A) wild type, (B) D_{LL}, and (C) D_{LL}-FY_LF_M. See text for further details.

charge-separated states on the L and M branches and differences in electronic couplings between the cofactors on the two branches. A working model for the relative free energies of the charge-separated states in wild-type RCs is given in Figure 2A and is derived from the following considerations. Calculations that account for the combined effects of a multitude of amino acid residues place $P^+B_L^-$ lower in free energy than $P^+B_M^-$ and similarly for $P^+H_L^-$ and $P^+H_M^-$.[50−54] Stark-effect and resonance Raman measurements indicate that a difference in the dielectric screening on the two branches also may contribute.[55−57] Additionally, calculations generally place the P^+B^- state higher in free energy than the P^+H^- state on both L and M branches by 0.15−0.25 eV, consistent with the difference in redox potentials of bacteriochlorophyll and bacteriopheophytin in vitro.[58−61] Calculations and experiments have provided estimates or bracketed ranges for the free energies of the charge-separated states in the wild-type RC: $P^+B_L^-$ 0.05−0.1 eV below P*;[29,50,51,62−70] $P^+H_L^-$ ∼0.25 eV below P* when relaxed;[71−75] $P^+B_M^-$ 0.1−0.2 eV above P* and $P^+H_M^-$ below P* by no more than ∼0.15 eV and probably within 0.1 eV.[50−52,76−79]

Systematic efforts to manipulate the free energy differences of the L- and M-branch charge-separated states by site-directed mutagenesis of key amino acids, including those near B_M and B_L, have led to mutant RCs in which electron transfer to the M branch competes effectively with charge separation to the L branch, yielding $P^+H_M^-$ (reviewed in ref 80). In one such strategy in *Rb. capsulatus* RCs, the symmetry-related Phe at L181 and Tyr at M208 were switched, following calculations that suggested that the tyrosine hydroxyl dipole in a particular orientation stabilizes the B_L anion (and by analogy, would do the same for the B_M anion).[50−52] Coupled with the change of Leu at M212 to a His (causing a BChl to be incorporated into the RC in place of H_L), this effort yielded the YFH mutant, in which $P^+H_M^-$ is formed with ∼30% yield.[79] Until recently this was the highest yield of this state obtained. Interestingly, the detergent-dependent heterogeneity of P* decay mentioned above for wild type is even more pronounced in YFH. The P* stimulated emission decay for YFH in LDAO can be reasonably fit by a monoexponential function yielding a 15 ps P* lifetime; however, for YFH in Deriphat the kinetics require the use of a biexponential function with time constants of 35 and 220 ps. Regardless of whether the detergent LDAO or Deriphat is used, the yield of M-side electron transfer in YFH is ∼30%. Subsequent $P^+H_M^- \rightarrow P^+Q_B^-$ electron transfer proceeds with a yield of ∼40% in the YFH mutant at room temperature.[81]

Efforts to characterize M-side electron transfer at low temperature have been limited, so we have little information on the temperature dependence of the rate or yield of $P^* \rightarrow P^+H_M^-$. In RCs that have various combinations of the mutations described above and also lack Q_A, low yields of $P^+Q_B^-$ have been reported mainly in photoaccumulation experiments between 10 and 100 K.[82−85] These studies indicate that both $P^* \rightarrow P^+H_M^-$ charge separation and $P^+H_M^- \rightarrow P^+Q_B^-$ electron transfer can occur at low temperature. Others have found that a signal due to electron transfer to H_M seen at room temperature diminishes at low temperature and interpreted the finding in terms of perturbation of the L-branch energetics with temperature[86] or that $P^* \rightarrow P^+H_M^-$ has an activation energy.[87,88] A weak temperature dependence of electron transfer to the M branch has been reported for the H(M182)L mutant, where a bacteriopheophytin denoted ϕ_B replaces B_M.[76] In this mutant P* decays to form $P^+H_L^-$ and $P^+\phi_B^-$ at both room and low temperature; electron transfer to $P^+H_M^-$ does not occur because $P^+\phi_B^-$ is apparently lower in free energy. The rate of $P^* \rightarrow P^+\phi_B^-$ charge separation was found to be essentially the same at 295, 77, and 9 K.

RCs devoid of H_L provide the best platform from which to assess quantitatively electron transfer to the M branch. Recently, we reported that $P^+H_M^-$ forms in ~70% yield at room temperature in the D_{LL}-FY_LF_M mutant,[89] which is based on the D_{LL} construct first reported by Youvan and co-workers and shown in their chromatophore studies[90,91] and in isolated RCs in our work[89] to be devoid of H_L. In D_{LL}, the D-helix residues M192−M217 that make contact with most of the cofactors on the photoactive L branch are replaced with the residues from L165−L190 (Figure 1). A *Rb. sphaeroides* RC that lacks H_M can be generated by a single bulky mutation, A(M149)W,[92] but this strategy does not work to selectively remove H_L in *Rb. capsulatus* RCs when nearby residues are converted to Trp (e.g., A(L120)W, J. I. Chuang et al., unpublished results). Remarkably, the crystal structure of the A(M149)W mutant displays only minor changes in protein structure despite the absence of the large H_M cofactor[93] suggesting that the same could be true for the structure of D_{LL}, which is devoid of H_L.

We reported that the P/P^+ potential in isolated D_{LL} RCs is at least 100 meV higher than in wild type.[89] On the basis of this finding, we proposed that all the charge-separated states (other than $P^+Q_A^-$ and $P^+Q_B^-$) are higher in frequency than P* (Figure 2B). From this model it follows that in D_{LL} charge separation does not compete with internal conversion of P*, which occurs with a time constant of ~180 ps (Deriphat) or ~100 ps (LDAO) at 295 K. We also showed in the D_{LL}-FY_LF_M mutant that two amino acid changes to D_{LL} [H(L168)F and H(M195)F; Figure 1B] together lower the P/P^+ potential to ~470 meV, which is comparable to the ~500 meV wild-type value. The third amino acid change in the D_{LL}-FY_LF_M mutant is F(L181)Y (Figure 1B), which places a Tyr residue near B_M. Therefore, the D_{LL}-FY_LF_M RC has (1) a dimer P with an oxidation potential similar to the wild-type value, (2) a Tyr at L181 that may stabilize $P^+B_M^-$, and (3) a Phe at M208 that may destabilize $P^+B_L^-$ (Figure 1B).

The proposed model for the free energies of the charge-separated states in D_{LL}-FY_LF_M is given in Figure 2C. Consistent with this model, we found that the P* lifetime in D_{LL}-FY_LF_M at 295 K is 55 ps and that P* decays via electron transfer to the M branch to give $P^+H_M^-$ in 70% yield, with ground-state recovery (assumed to be by direct P* → P internal conversion) accounting for the remaining 30% of P* decay. These data give a rate constant for electron transfer from P* to $P^+H_M^-$ of $0.7/(55\text{ ps}) = (78\text{ ps})^{-1}$, which is a factor of about 20 slower than the formation of $P^+H_L^-$ in wild type and is presumed to be superexchange-mediated by $P^+B_M^-$. In the present paper we report measurements of D_{LL} and D_{LL}-FY_LF_M at 77 K that complement our previous room-temperature measurements. The complexity of the data leads us to consider a series of models involving homogeneous or heterogeneous populations of RCs in order to understand better the underlying physical phenomena. The goal of these studies is to obtain further information on the relative free energies of the charge-separated states in these mutants and the temperature dependence of electron transfer from P* to the M-branch cofactors.

Experimental Methods

Reaction Center Growth and Purification. Wild-type, D_{LL}, and D_{LL}-FY_LF_M RCs were expressed, isolated, and purified using the detergent Deriphat 160-C as described previously.[89] For measurements of D_{LL} RCs in LDAO, the detergent was exchanged to LDAO after initial Deriphat 160-C purification. Due to extremely low yields, D_{LL}-FY_LF_M was not subjected to buffer exchange and so was not examined in LDAO. Glycerol was added to RCs in 10 mM Tris pH 8, 0.05% Deriphat 160-C, or 10 mM Tris pH 8, 0.05% LDAO, to a final concentration of 60% glycerol (v/v) for low-temperature experiments unless otherwise indicated and will be referred to as RC in Deriphat glass or LDAO glass, respectively.

Picosecond Fluorescence Measurements. The fluorescence decay of P* was measured by fluorescence upconversion essentially as described.[94] Emission was detected at 890 nm at the magic angle relative to the excitation at 800 nm. RC samples had an OD of 0.6 at 800 nm in a 1 mm path length and contained 1 mM dithionite and terbutryn at 30 times the RC concentration to reduce Q_A and displace Q_B, respectively. Samples were held in a quartz cuvette in an MMR refrigerator (MMR Technologies) and cooled with argon to 140 K. Data were collected to 1.3 ns for each scan, and the cuvette position was rastered after each time scan. Between 10 and 40 scans were averaged for each sample. Each average was fit to the convolution of the pump−probe cross correlation as determined the same day (typically between 150 and 170 fs) and a sum of exponentials, which included a fixed rise time of 150 fs due to the energy transfer from B* to P.[94]

Picosecond Transient Absorption Spectroscopy. The transient absorption measurements were conducted basically as described previously[95] and utilized a regeneratively amplified Ti:sapphire laser pumping an OPA (Spectra Physics) to generate 130 fs excitation and white-light probe flashes at 10 Hz. For experiments probing the visible region of the spectrum (500−700 nm) the RCs samples had an OD of 1 at 860 nm (at 295 K) in a 2 mm path length and were excited with ~20 μJ excitation flashes at 870 nm. For experiments probing the near-infrared region (820−1000 nm), the RC samples had an OD of 0.5−0.6 at 860 nm (at 295 K) in a 2 mm path length and were excited with ~20 μJ excitation flashes at 595 nm. The induced absorption changes for both 870 and 595 nm excitation were verified to be linear and subsaturating with 20% of the RCs typically excited. The D_{LL}-FY_LF_M samples contained terbutryn at 25−30 times the RC concentration, and sometimes additionally contained 1 mM sodium dithionite. No differences between the results were found as a function of the presence or absence of dithionite. The relative polarization of the excitation and probe flashes was at the magic angle. The RCs were held in a 2 mm plastic cuvette and cooled in the dark to 77 K in an Oxford Instruments cryostat. In some cases a small (≤5%) signal "before zero-time" was observed, representing a fraction of the RCs that had not recovered to the ground state between the 10 ms separation of successive excitation flashes (10 Hz repetition rate); the small pre-zero-time signal was ignored in data analysis.

The transient absorption changes were monitored simultaneously (on a dual diode array detector) over an ~220 nm wide window following each excitation flash. The ΔA spectra were recorded as a function of pump−probe delay time, with each spectrum representing the average of ~150 excitation flashes. Such spectra were acquired as a function of pump−probe delay time from several picoseconds "before zero-time" to as long as 3.5 ns, with 60−100 spectra constituting a typical data set. Two or three such data sets, each one acquired on a fresh sample on a different day, were collected for both the 500−700 nm (Q_X and anion) probing region and the 850−1050 nm (Q_Y and stimulated emission) probing region. These data sets were then subject to several different fitting methods. First, kinetic data (time, ΔA pairs) were generated by averaging the ΔA over 3−5 nm intervals for each spectrum (as a function of delay time) in a data set. A time profile for the ΔA within such a 3 or 5 nm interval is referred to herein as single-wavelength kinetics. These data were fit to either a single-exponential function (the

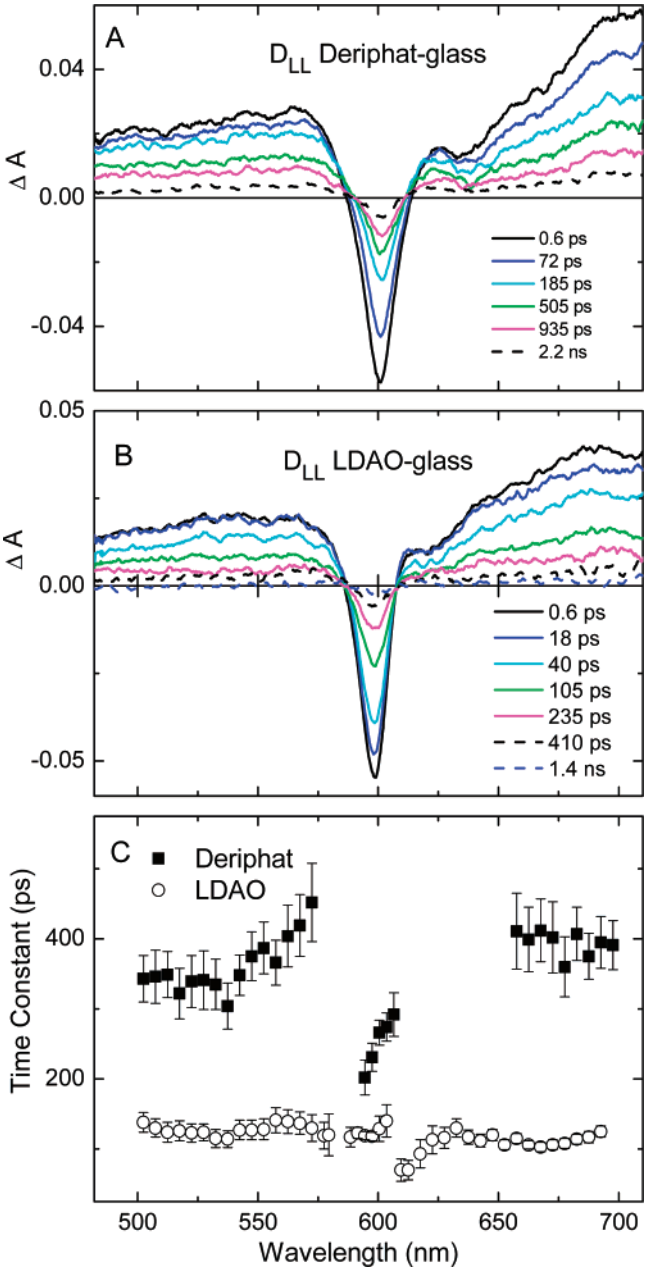

Figure 3. 77 K transient absorption difference spectra for D_{LL} Deriphat-glass RCs (A) and D_{LL} LDAO-glass RCs (B) acquired in the visible region spectrum at the times indicated following a 130 fs, 870 nm excitation flash. (C) Time constants resulting from fitting the single-wavelength kinetic data for D_{LL} Deriphat glass (solid squares) and D_{LL} LDAO glass (open circles) to a single-exponential function. See text for further details.

convolution of the instrument response with one exponential plus a constant) or a biexponential function (the convolution of the instrument response with two exponentials plus a constant). Second, the as-acquired spectra comprising the Q_X region and Q_Y regions were subjected to global kinetic and spectral analysis using routines written in Igor Pro 6.01 (Wavemetrics).

Results

D_{LL} RCs in Deriphat Glass. Excitation of D_{LL} in Deriphat glass or LDAO glass with 870 nm 130 fs flashes produces the lowest singlet excited state of the dimer, P*, characterized in the visible region by the 0.6 ps spectrum shown in Figure 3, parts A and B, respectively. The transient absorption difference spectrum of this state displays a broad, mostly featureless P* absorption between 500 and 700 nm, bleaching of the Q_X band of P (maximum at 601 nm in Deriphat and 598 nm in LDAO), and a shallower dip just to the red of the Q_X bleaching (near 635 nm in Deriphat and 620 nm in LDAO). The 635 or 620 nm feature may represent bleaching of a weak ground-state absorption band of P (to a high-energy Q_Y excited state) that has been calculated to lie in this region.[96] These spectral features change shape little with time, including the persistence of two isosbestic points at $\Delta A \sim 0$ flanking the Q_X P bleaching for LDAO glass (but not Deriphat glass), and decay nearly to $\Delta A = 0$ over the time course shown. These findings indicate that return of P* to the ground state is essentially complete by 2 ns. There is perhaps a few percent yield of the triplet excited state of P (^{3}P) as evidenced by the residual 600 nm bleaching at >1 ns.

The single-wavelength ΔA changes between 500 and 700 nm were individually fit to a function containing either one or two exponentials as detailed in the Experimental Methods section. For the single-exponential fits, the resulting time constants vary as a function of probe wavelength (Figure 3C), with average values of 360 ± 70 ps in Deriphat glass and 120 ± 20 ps in LDAO glass. The double-exponential fits gave average time constants of 130 ± 50 and 600 ± 190 ps in Deriphat glass and 50 ± 52 and 330 ± 110 ps in LDAO glass.

Figure 4, parts A and B, shows transient absorption difference spectra between 820 and 1000 nm for D_{LL} in Deriphat glass and LDAO glass, respectively, as a function of time following excitation with a 600 nm 130 fs flash. The 0.6 ps spectrum is characterized by bleaching of the long-wavelength absorption band of P at 875 nm with stimulated emission from P* giving rise to a negative ΔA at longer wavelengths. This overall spectral shape, including the prominent stimulated emission centered at 925 nm, persists as the features decay nearly to $\Delta A = 0$. As in the Q_X absorption region, these observations indicate that by 2 ns P* has returned to the ground state, except for perhaps a few percent yield of ^{3}P represented by the residual bleaching in the 3 ns spectrum.

The single-wavelength ΔA time profiles spanning 825−980 nm were fit as above to a single-exponential function. The apparent P* lifetime shows a significant variation as a function of wavelength (Figure 4C), ranging in this spectral region from 220 to 380 ps for D_{LL} in Deriphat glass and from 120 to 240 ps in LDAO glass. In Figure 5, two representative time profiles for the Deriphat-glass sample underscore the wavelength dependence reflected by the solid squares in Figure 4C. The fit time constant is 273 ± 13 ps at 840−845 nm and 365 ± 11 ps at 920−925 nm. At 885−890 nm an intermediate value of 323 ± 7 ps is found. This value compares well to P* lifetime determined in this medium by spontaneous fluorescence decay, which yields a time constant of 293 ps for the dominant (81%) phase of the observed biexponential decay at 890 nm and 140 K. A faster 12 ps component (19%) was also observed in the spontaneous fluorescence measurements but was not seen in the 77 K transient absorption measurements and so was not considered further. The average time constant from the single-exponential fits of the transient absorption data in Deriphat glass over the entire region between 825 and 980 nm is 300 ± 40 ps, in good agreement with the 360 ± 70 ps average P* lifetime measured in the Q_X region. Table 1 (column 3) lists the 330 ± 60 ps value that is the average of the single-exponential fits from the Q_X (500−700 nm) and Q_Y (825−980 nm) regions for D_{LL} in Deriphat glass. The average value for the Q_X plus Q_Y regions for LDAO glass is 150 ± 40 ps.

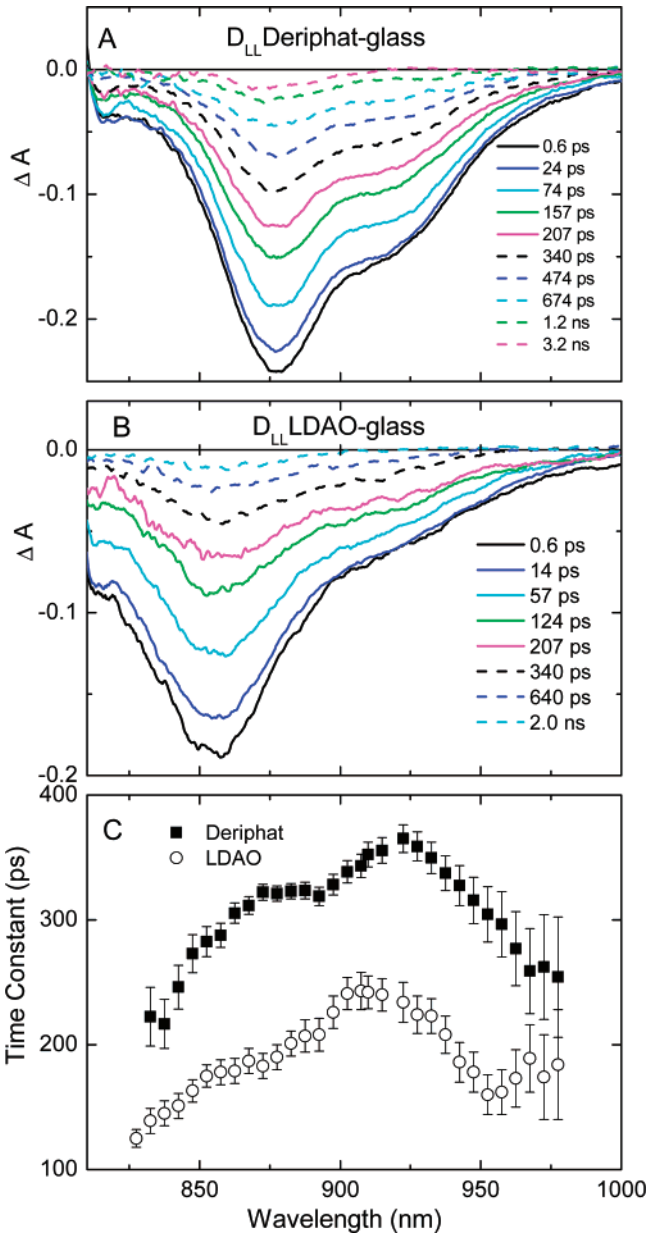

Figure 4. 77 K transient absorption difference spectra for D_{LL} Deriphat-glass RCs (A) and D_{LL} LDAO-glass RCs (B) acquired in the region of the Q_Y absorption band of P at the times indicated following a 130 fs, 595 nm excitation flash. (C) Time constants resulting from fitting the single-wavelength kinetic data for D_{LL} Deriphat glass (solid squares) and D_{LL} LDAO glass (open circles) to a single-exponential function. See text for further details.

The single-wavelength ΔA time profiles from the Q_Y region were also fit to a biexponential function. These fits for D_{LL} in Deriphat glass give average time constants of 180 ± 60 and 430 ± 60 ps, which again compare favorably with the 130 ± 50 and 600 ± 190 ps determined from biexponential fits of the Q_X data. The analogous fits for D_{LL} in LDAO glass give average time constants of 140 ± 50 and 500 ± 170 ps, which also compare well with the biexponential fits of the Q_X data. Averaging the time constants over the Q_Y and Q_X regions gives time constants of 150 ± 60 and 520 ± 170 ps for Deriphat glass and 90 ± 50 and 390 ± 160 ps for LDAO glass (Table 1, columns 4 and 5). The P* lifetime for D_{LL} in chromatophores at 80 K has been reported as 500 ± 100 ps by transient absorption at 525 nm, and 440 (70%) and 840 ps (30%) by fluorescence at 920 nm,[97] in good agreement with the longer-lived component observed here for D_{LL} RCs in 77 K Deriphat glass.

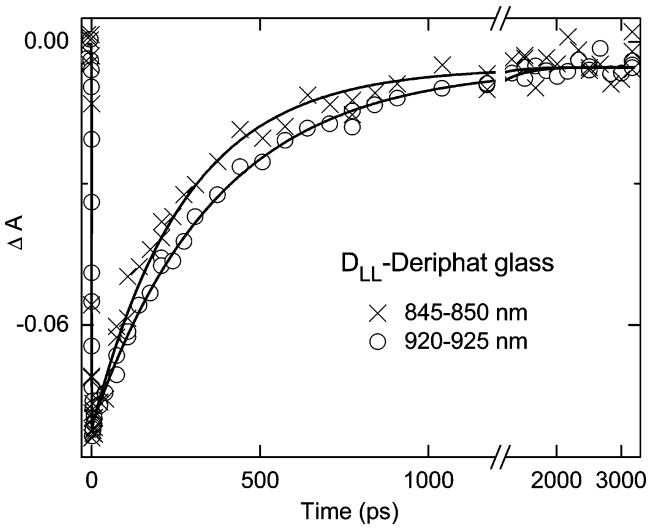

Figure 5. Decay of the P bleaching averaged between 845 and 850 nm (×) and decay of the stimulated emission averaged between 920 and 925 nm (○) for D_{LL} Deriphat-glass RCs at 77 K. The data have been normalized to the same total ΔA span for presentation purposes. The solid lines are fits to a single-exponential function giving time constants of 273 ± 13 ps (845−850 nm) and 365 ± 11 ps (920−925 nm).

TABLE 1: Time Constants for P* Decay in D_{LL} RCs at 77 K

		1-exponential	2-exponential	
medium	analysis	τ (ps)	τ1 (ps)	τ2 (ps)
Deriphat	local[a]	330 ± 60	150 ± 60	520 ± 170
	global[b]	330 ± 20	160 ± 20	430 ± 20
LDAO	local[a]	150 ± 40	90 ± 50	390 ± 160
	global[b]	170 ± 10	80 ± 10	300 ± 20

[a] Average from individual single-wavelength fits (time profiles of ΔA averaged over 3 or 5 nm intervals and spanning the visible (Q_X) and Q_Y regions; see the Results section). [b] From global fits of combined Q_X and Q_Y data.

Global Analysis for D_{LL} RCs at 77 K. Global analysis was performed on the combined data from the Q_X (500−700 nm) and Q_Y (820−1000 nm) regions for D_{LL} RCs in both Deriphat glass and LDAO glass. First, the combined data from the Q_X and Q_Y regions were fit globally to a single-exponential function. This analysis returned values of 330 ± 20 ps for D_{LL} in Deriphat glass and 170 ± 10 ps for LDAO glass (Table 1, column 3). As expected, these values are essentially the same as the average values determined from the single-wavelength fits (Table 1, column 3). Second, the data were globally fit to a biexponential function, which gave time constants of 160 ± 20 and 430 ± 20 ps for D_{LL} in Deriphat glass and 80 ps ± 10 and 300 ± 20 ps for D_{LL} in LDAO glass (Table 1, columns 4 and 5). These pairs of values compare very well to the pairs of average values determined from the single-wavelength biexponential fits (Table 1, columns 4 and 5). Further analysis and modeling of D_{LL} RCs at 77 K in terms of a heterogeneous population of two different forms of P* are given in the Discussion section.

Overview of Results and Analysis for D_{LL}-FY_LF_M RCs. Subpicosecond time-resolved transient absorption data for D_{LL}-FY_LF_M at 77 K in Deriphat glass are shown in Figures 6−8. The data are more complex than those found previously for this mutant at room temperature.[89] Cursory examination of the transient absorption spectra in Figure 8A reveals that a

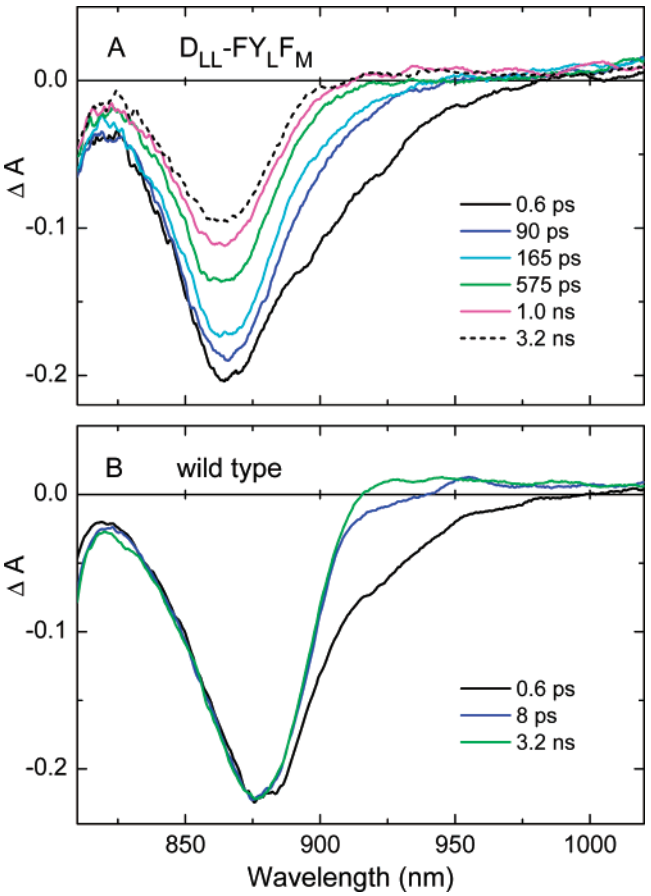

Figure 6. Comparison of the 77 K transient absorption difference spectra for D_{LL}-FY_LF_M Deriphat-glass RCs (A) and wild-type Deriphat-glass RCs (B) acquired in the region of the Q_Y absorption band of P at the times indicated following a 130 fs, 595 nm excitation flash.

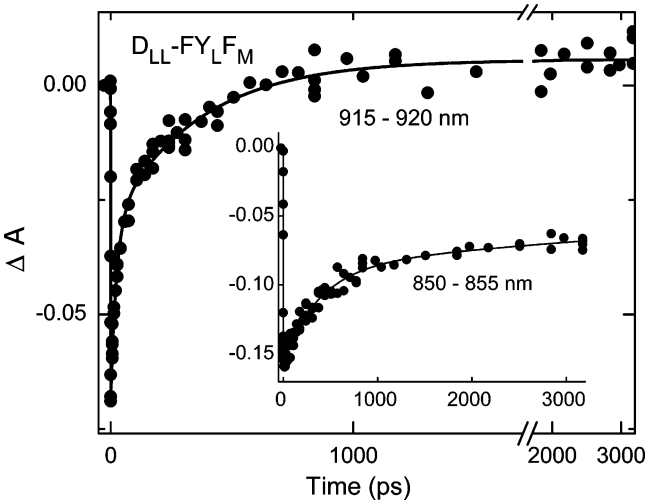

Figure 7. Kinetic data and fits for D_{LL}-FY_LF_M Deriphat-glass RCs at 77 K. The main panel shows decay of the stimulated emission averaged between 915 and 920 nm (●) and fit to a biexponential function (solid line). The inset shows decay of the P bleaching averaged between 850 and 855 nm (●) and fit to a biexponential function (solid line). See text for further details.

significant bleach occurs in D_{LL}-FY_LF_M in the Q_X band of H_M at 529 nm, whereas only a small negative signal, possibly a small bleach, is observed in this region in wild type; instead the well-known bleach of the Q_X band of H_L at 546 nm is observed (Figure 8B). The wild-type data reflect an essentially 100% yield of the $P^+H_L^-$ state, whereas the relative yield (scaled

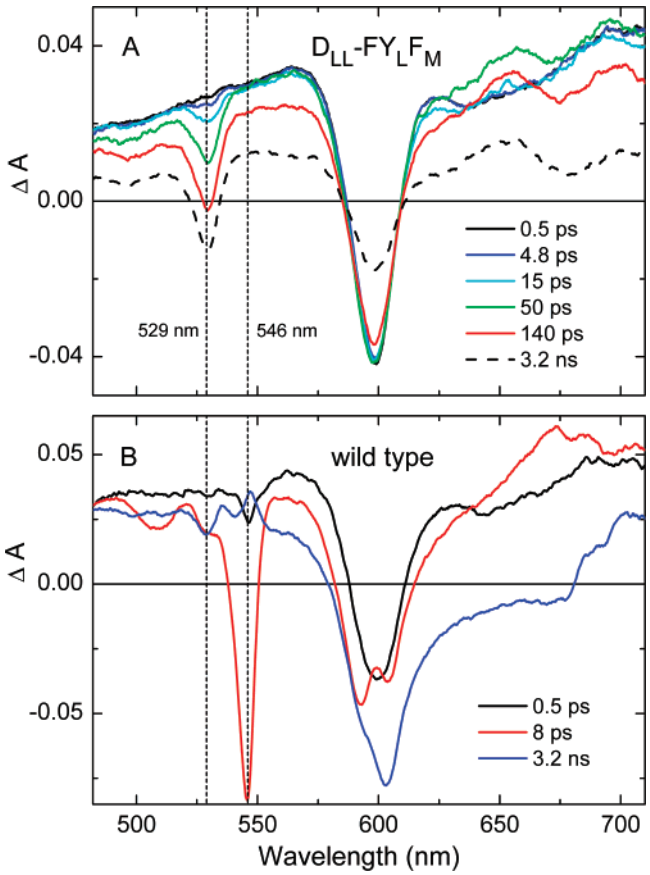

Figure 8. Comparison of the 77 K transient absorption difference spectra for D_{LL}-FY_LF_M Deriphat-glass RCs (A) and wild-type Deriphat-glass RCs (B) acquired in the visible region of the spectrum at the times indicated following a 130 fs, 870 nm excitation flash.

to the bleach of the P Q_X band) is considerably smaller for $P^+H_M^-$ in D_{LL}-FY_LF_M. Furthermore, the bleach of the Q_X band of H_M in D_{LL}-FY_LF_M is smaller than what was observed earlier at room temperature (Figure 4A in ref 89). Thus, $P^+H_M^-$ is being formed at low temperature, but either its yield, per P excited, is lower than at room temperature or some fraction of P* is not forming $P^+H_M^-$ at all. These qualitative observations lead naturally to the consideration of models for heterogeneity that then permits quantitative analysis of the yields and rates. Following the introduction of two possible models, transient absorption data in the near-infrared Q_Y and then visible Q_X regions are presented along with detailed data analysis based on *one* of these models. The implications of this analysis for processes occurring in D_{LL}-FY_LF_M, D_{LL}, and wild type are described further in the Discussion section. It will be seen that regardless of the complexities and model chosen, electron transfer from P* to the M side is found to have a weak temperature dependence and thus to be an effectively activationless process.

Two basic models are distinguished as heterogeneous and homogeneous with respect to the initial population of P*. Both models have been discussed previously for the YFH mutant in Deriphat at 295 K.[39] In the heterogeneous-RC model of D_{LL}-FY_LF_M RCs in Deriphat glass at 77 K, we propose there are at least two distinct and uncoupled populations having different forms of P* whose fates are very different. These populations could differ in characteristics such as the electronic structure of P*, the electronic couplings for electron transfer to H_M, and the free energies of the charge-separated states. With respect to this model, the data described below can be reconciled with

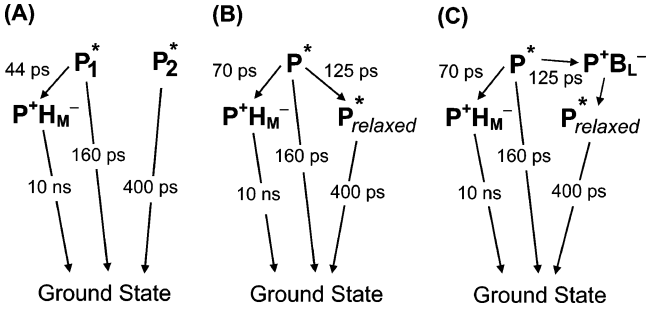

Figure 9. Models for charge separation in the D_{LL}-FY_LF_M RC in Deriphat glass at 77 K: heterogeneous-RC model (A) and two variants of a homogeneous-RC model (B and C). The internal conversion rate constant of $(160\ ps)^{-1}$ for the photoactive P_1* fraction in (A) and for the initial form of P* in (B) and (C) is assumed to be the same as the shorter-lived component of the P* decay for the D_{LL} RC in Deriphat glass at 77 K. Similarly, the rate constant of $(400\ ps)^{-1}$ for the inactive P_2* population in (A) and for the relaxed form of P* in (B) and (C) is assumed to be the same as the longer-lived component of P* decay and ground-state recovery for D_{LL}-FY_LF_M at 77 K. The parameters shown give a lifetime of P_1* in (A) and P* in (B) and (C) of 35 ps, which is the measured value. The calculated yield of $P^+H_M^-$ using the parameters shown is 80% for the photoactive subpopulation (P_1*) in (A) and 50% for the entire P* initial population in (B) and (C).

the following: (1) in approximately half of the RCs P* decays by electron transfer to the M branch to give $P^+H_M^-$, and (2) in the remaining half, P* decays by deactivation to the ground state. Within the heterogeneous model, the raw transient absorption spectra reflect the *sum* of the absorption changes arising from these two subpopulations in which very different and kinetically uncoupled photochemical events occur, as reflected in Figure 9A.

In alternative homogeneous models (Figure 9, parts B and C), P* decays with roughly 50/50 yields via electron transfer to H_M and via formation of an inactive, or "dead-end" state. "Dead-end" implies that this state cannot do subsequent electron transfer to H_M (and clearly not to H_L, which is absent) but instead decays only to the ground state. An example of such an inactive state is a relaxed form of P* produced from the initial form of P* (Figure 9B) or produced from a charge-separated state such as $P^+B_L^-$ (Figure 9C). In both the models shown in Figure 9, parts B and C, direct decay of the initial form of P* to the ground state is less effective than the two alternative pathways.

Throughout the following, the results for D_{LL}-FY_LF_M in Deriphat glass are presented in terms of the heterogeneous-RC model. Doing so allows connections to be drawn between the data for both D_{LL}-FY_LF_M and D_{LL} and leads to a model that is consistent for both mutants. Further analysis and comparisons of these data in terms of the heterogeneous- and homogeneous-RC models are given in the Discussion section.

Time Evolution of Near-Infrared Spectra for D_{LL}-FY_LF_M in Deriphat Glass at 77 K. Spectra acquired at several delay times (0.6 ps to 3.2 ns) in the P-bleaching region for D_{LL}-FY_LF_M and wild type in Deriphat glass at 77 K are shown in Figure 6, parts A and B, respectively. The data for wild type reflect ~100% conversion of P* → $P^+H_L^-$ → $P^+Q_A^-$ with ~2 and ~100 ps time constants, respectively. Whereas the magnitude of P bleaching in wild type is constant on this time scale, in D_{LL}-FY_LF_M there is extensive decay of P bleaching (835−865 nm) at 3.2 ns compared to 0.6 ps. A representative P* stimulated emission decay profile (data averaged between 915 and 920 nm) and fit to a biexponential function for D_{LL}-FY_LF_M are shown in Figure 7 (main panel). (Note that assignment of this data to stimulated emission is valid because little if any contribution from P-bleaching decay is expected at these wavelengths, as is evident for wild type in Figure 6B.) Similar biexponential fits to the single-wavelength time profiles between 915 and 935 nm give average time constants of 32 ± 7 and 380 ± 70 ps. These results are in good agreement with the P* kinetics measured independently by P* spontaneous fluorescence, the majority of which decays with time constants of 22 and 282 ps at 890 nm and 140 K. Approximately 20% of the fluorescence amplitude arises from an additional 1.7 ps time constant that was not seen in the transient absorption data and was not considered further. Within the heterogeneous model, these observations are evidence for at least two populations of P* in D_{LL}-FY_LF_M, one with a lifetime of several hundred picoseconds (similar to that observed for D_{LL} in Deriphat glass) and one with a lifetime that is only tens of picoseconds.

To examine the kinetics of P-bleaching decay in D_{LL}-FY_LF_M, the absorption changes on the blue side of the P bleaching between 835 and 865 nm were analyzed. At these wavelengths there is little if any contribution from P* stimulated emission (see wild-type data in Figure 6B). A representative time profile (850−855 nm) is shown in Figure 7 (inset) along with a fit to a biexponential function. The constant value was fixed at $\Delta A = 0$ since no long-term charge separation can occur; neither long-lived state $P^+Q_A^-$ nor $P^+Q_B^-$ can form in the absence of H_L and the presence of excess terbutryn, which displaces Q_B. The same results were obtained for D_{LL}-FY_LF_M RCs containing both a 25-fold excess of terbutryn and 1 mM sodium dithionite; the latter chemically reduces Q_A and Q_B. The average time constants determined from single-wavelength time profiles between 835 and 865 nm are 410 ± 60 ps and ~10 ns (range 5−15 ns), each with a ~50% amplitude. Inclusion of a third exponential, either as a free parameter or with a fixed value between 20 and 50 ps, yielded only small amplitudes (≤5%) for this component and did not significantly improve the fits.

Within the heterogeneous-RC model these results indicate that in roughly 50% of the D_{LL}-FY_LF_M RCs in Deriphat glass, the ultimate fate of P* is similar to that found in D_{LL}. In this fraction P* decays to the ground state with an average time constant of ~400 ps, as is evident from the P bleaching and P* stimulated emission decay kinetics. In the other 50% of the RCs, P* decays in ~35 ps and produces a state with a lifetime of roughly 10 ns. This product is identified as $P^+H_M^-$ based on the time evolution of the Q_X region spectra presented in the next section.

Time Evolution of Visible Spectra for D_{LL}-FY_LF_M in Deriphat Glass at 77 K. For D_{LL}-FY_LF_M, the spectrum acquired in the Q_X region 0.5 ps after excitation (Figure 8A) is again similar to the 0.6 ps spectrum of D_{LL} (Figure 3A) and wild type (Figure 8B), and assigned to P*. [A small caveat is that in wild type the onset of H_L bleaching at 546 nm is captured at 0.5 ps because the P* lifetime at 77 K is only 1.9 ± 0.2 ps (kinetic data not shown).] In the spectra of D_{LL}-FY_LF_M at later times there is prominent bleaching at 529 nm, which can be assigned to bleaching of the Q_X ground-state band of H_M, and a prominent absorption band with a peak near 650 nm, which can be assigned to the H_M anion. These spectral features are consistent with formation of $P^+H_M^-$. They parallel, but are blue-shifted from, the 546 nm Q_X bleaching of H_L and 670 nm peak of the H_L anion band observed in the $P^+H_L^-$ spectrum of wild type at 8 ps (Figure 8B). Note that there is no indication of H_L bleaching in D_{LL}-FY_LF_M, consistent with the absence of this pigment in these RCs. The blue shift of the Q_X and anion bands of H_M compared to H_L is expected and has been shown to derive largely from the hydrogen bond between the H_L ring-V keto

group and E(L104), whereas the symmetry-related V(M131) cannot donate an analogous hydrogen bond to H_M.[98−101] The Q_X bleaching of H_M in D_{LL}-FY_LF_M has a full width at half-maximum (fwhm) about 2 nm larger than that of the Q_X band of H_L in wild type (11 vs 9 nm). These width differences are consistent with the ground-state absorption features at 77 K, which have estimated fwhms of 11 nm (for H_M in D_{LL}-FY_LF_M) and 8.5 nm (for H_L in wild type).

The bleaching at 529 nm develops with an ∼35 ps time constant (data not shown), which matches well the shorter component of the P* stimulated emission kinetics (32 ± 7 ps). Within the heterogeneous model this 35 ps component can be assigned to the P* lifetime for the 50% of the D_{LL}-FY_LF_M RCs in which electron transfer to the M side occurs, yielding $P^+H_M^-$. In contrast, there is no evidence (<10% amplitude) for a 35 ps component in the decay kinetics of the 600 nm bleaching. Rather, the bleaching of the Q_X band of P decays biexponentially with time constants of ∼380 and ∼10 ns, both with ∼50% amplitude (data not shown). The same result is observed for P-bleaching decay in the Q_Y spectral region. Because P-bleaching decay represents ground-state recovery, a 35 ps kinetic component in the P ground-state absorption region would reflect competing P* deactivation to the ground state in the photoactive population of P*. Because the 35 ps component is absent from the Q_X and Q_Y P-bleaching decay kinetics, we conclude that P* → $P^+H_M^-$ occurs with high yield in this 50% population. Estimates of the yield based on these and other data are presented in the Discussion section.

Comparing the spectra at 140 ps and 3.2 ns in Figure 8A, the magnitude of bleaching at 529 nm, when referenced to the positive absorption on either side of the peak, is little changed, indicating that $P^+H_M^-$ is fully populated by 140 ps and persists for >5 ns. This is consistent with $P^+H_M^-$ formation with a 35 ps time constant and $P^+H_M^-$ decay by charge recombination to the ground state with a time constant on the order of 10 ns. A qualitative examination of these two spectra also provides a useful consistency check for the heterogeneous model. Within this model, a given transient spectrum should be the sum of the predicted absorption changes due to the 50% population of RCs in which P* → $P^+H_M^-$ has occurred in high yield and the 50% population of RCs in which P* deactivates only to the ground state. A 140 ps delay time corresponds to four 1/e times of the 35 ps P* lifetime for the photoactive fraction and thus to a maximum population of $P^+H_M^-$. Therefore, one would expect maximal 529 nm bleaching of the Q_X band of H_M and maximal 650 nm absorption of the anion band of H_M. In contrast only minimal decay of the 600 nm P bleach is predicted because (1) the high yield of $P^+H_M^-$ precludes significant P ground-state recovery in the photoactive fraction and (2) P* decays to the ground state with a slow 400 ps constant in the nonphotoactive fraction. The 140 ps transient spectrum agrees with both of these predictions (Figure 8A).

The spectrum acquired at a 3.2 ns delay (Figure 8A) can be interpreted similarly. Within the heterogeneous model, by this time the absorption changes will have taken on different relative magnitudes of these same features. Both the 529 nm H_M bleach and the 650 nm H_M anion absorption band are of similar overall shape and amplitude (as measured against the overlapping positive absorption from P*) at 3.2 ns as at 140 ps, consistent with a ∼10 ns lifetime for $P^+H_M^-$. In contrast, between 140 ps and 3.2 ns significant fractions of both the broad, positive P* transient absorption and the 600 nm P bleaching have decayed. This is consistent with P* → ground state deactivation with a 400 ps time constant in the 50% nonphotoactive fraction of P*. Thus, the spectrum remaining at 3.2 ns arises exclusively from $P^+H_M^-$.

Global Analysis for D_{LL}-FY_LF_M in Deriphat Glass. Global analysis of the combined Q_X (500−700 nm) and Q_Y (825−1000 nm) data was performed as described for D_{LL}, except that the data were fit to three exponentials plus a constant (convolved with the instrument response). The analysis was carried out for the heterogeneous model described above and gave time constants of 35 ± 3 ps, 410 ± 30 ps, and 10 ± 1 ns. As expected from the model, the species-associated spectra for the 35 ps and 410 ps components (two forms of P*) are similar overall to the raw spectrum (Figures 6A and 8A) at 0.5 or 0.6 ps except for differences in the relative amplitudes of the stimulated emission and bleaching features. The species-associated spectrum of the 10 ns component ($P^+H_M^-$) is similar to the raw spectrum at 3.2 ns. Like the analysis in the preceding section, the global analysis is consistent with the presence of two roughly equal subpopulations of RCs. Both analyses support a model in which a photoactive fraction exhibits a 35 ps decay of P* to $P^+H_M^-$ in high yield and subsequent $P^+H_M^-$ → ground state charge recombination with an ∼10 ns time constant, whereas the other fraction is characterized by ∼400 ps deactivation of P* only to the ground state.

Discussion

Heterogeneous-RC Model for D_{LL}. Complex spectral evolution in bacterial RCs, both wild type and a variety of mutants, is well documented, taking different forms in different types of measurements. These include the following: (1) *detection*-wavelength-dependent time constants determined from transient absorption measurements for both P* → $P^+H_L^-$ charge separation (involving $P^+B_L^-$ as a discrete or superexchange intermediate or both) and $P^+H_L^-$ → $P^+Q_A^-$ electron transfer in wild-type RCs at both room and low temperature,[15,16] (2) transient absorption measurements showing *excitation*-wavelength-dependent kinetics,[37,102,103] (3) biexponential P* stimulated emission decay kinetics as measured by transient absorption,[14,17,18,20,22,31,35,46] and (4) biexponential or multiexponential P* spontaneous fluorescence decay kinetics in wild type and mutants.[19,23,24,30,35,45] Various models for these phenomena have been discussed, often in terms of multiple RC forms or a distribution of RC forms, each form having a slightly different P* lifetime (or rate of $P^+H_L^-$ → $P^+Q_A^-$ electron transfer), such that the ensemble yields complex kinetic profiles. Static heterogeneity could arise from RCs that differ in distances between cofactors, the nature and strengths of cofactor−protein interactions, or a host of similar factors that affect either the electronic or Frank−Condon contribution (free energy gaps between the relevant states) to the rates of the electron-transfer processes. Contributions to complex kinetic profiles from dynamic effects involving motions of the chromophores, the protein, or both accompanying or following the decay of P* or $P^+H_L^-$ also have been discussed.[18,22,65,74,104−107]

In our previous work, we proposed the scheme for D_{LL} given in Figure 2B, wherein the charge-separated intermediates (states other than $P^+Q_A^-$ and $P^+Q_B^-$) lie above P* in free energy. This scheme derived from (1) the current view of the free energies of the intermediates in wild type, (2) the measured P/P^+ potential in D_{LL} being at least 100 meV higher than in wild type, and (3) the lack of spectral signatures for formation of a charge-separated state from P* in D_{LL} at 295 K. In the simplest interpretation, the data presented here for D_{LL} in either Deriphat glass or LDAO glass at 77 K are similar to the results for D_{LL}

at 295 K and can be reconciled with the model shown in Figure 2B, namely, with the charge-separated intermediates lying above P* and P* → ground state (via internal conversion) being the only decay route of P*. This simple framework for the time evolution of the spectra in Figures 3 and 4 follows from the clear persistence of P* stimulated emission throughout the entire several hundred picoseconds during which the RC returns to the ground state. In this regard the D_{LL} RC presents an unprecedented opportunity to examine the spectral evolution of P* decay across the entire spectrum precisely because it is not capable of electron transfer; the P bleach decay and P* stimulated emission decay are indicative of the *same* process, P* → P.

Within the energy scheme illustrated in Figure 2B, the observed probe-wavelength dependence of the P* lifetime in D_{LL} at 77 K (Figures 3C and 4C) requires, at the least, a heterogeneous model involving two subpopulations of P* with different lifetimes. As noted in the Introduction, the possibility that that there may be different forms of P* and/or P in an RC sample is reasonable and supported by observed changes in various RC or cofactor properties as a function of milieu. For example, the long-wavelength absorption band of P in D_{LL} is ∼20 nm blue-shifted in LDAO compared to Deriphat at both room and low temperature. The near-infrared absorption band of P in wild type and many mutants has similarly been shown to vary widely with conditions (such as pH or detergent) indicating that the protein environment can affect the spectral/electronic properties of P. Even in the absence of a wavelength-dependent P* lifetime, the difference in the average P* lifetime of D_{LL} in LDAO versus in Deriphat (110 vs 180 ps at 295 K[89] and 150 vs 330 ps at 77 K) strongly suggests that different forms of P* (and/or P) exist in these samples.

The results of global analysis using a biexponential fit to the combined visible and near-infrared data sets for D_{LL} in Deriphat glass or LDAO glass are consistent with a heterogeneous-RC model, in which at least two subpopulations of P* decay in parallel with distinct lifetimes (Figure 9A). These two subpopulations are denoted as the shorter-lived and longer-lived forms of P*. Noteworthy aspects of the global analysis are as follows: (1) in Deriphat glass all the species-associated spectra show the same prominent features evident in the as-acquired spectra (Figures 3A and 4A), and the same holds true in LDAO glass (Figures 3B and 4B); (2) the amplitude ratio of P* stimulated emission versus P bleaching is smaller for the shorter-lived form of P* than for the longer-lived form of P*, and this effect is more pronounced for D_{LL} in LDAO than in Deriphat; (3) both forms of P* have a shorter lifetime in LDAO than in Deriphat, with the difference more pronounced for the shorter-lived form (Table 1); (4) a larger fraction of the sample (an additional ∼15%) is in the shorter-lived P* form than in the longer-lived form in LDAO versus Deriphat. In summary, these differences can be understood if the shorter-lived P* form in either detergent is less emissive than the longer-lived form, if nonradiative deactivation of P* is enhanced for D_{LL} in LDAO compared to Deriphat, and if the fraction of P* in the shorter-lived form is larger in LDAO than in Deriphat.

The temperature dependence of the P* decay profiles also likely is rooted in differences in the relative populations of different forms of P*. We note that the 180 ps P* lifetime for D_{LL} in Deriphat at 295 K is comparable to the 160 ps lifetime of the shorter-lived P* form in Deriphat glass at 77 K (Table 1). Similarly, the 110 ps lifetime for P* D_{LL} in LDAO at 295 K is comparable to the 80 ps lifetime of the shorter-lived P* form in LDAO glass at 77 K. Longer-lived P* forms were not resolved at room temperature. One possibility is that both P* forms are present at 295 K but have similar photophysical properties such that they are not readily distinguished in the transient absorption measurements. At low temperature then, the shorter-lived form retains a lifetime comparable to, but perhaps slightly faster than, at room temperature, while the lifetime of the longer-lived form is substantially lengthened. The relative proportions of the two subpopulations may also change as a function of temperature, and one possibility consistent with the data is that the proportion of the longer-lived form increases at low temperature. In the extreme case, P* exists in only one form or rapidly interconverting forms at room temperature but freezes into two different forms at low temperature where barriers for interconversions between the forms cannot be overcome, as has been postulated for other RCs.[24,25,43,100]

Finally, we consider possible physical differences between the two forms of P*. One is medium-induced alterations in the electrostatic environment (or structure) of P that modulate its electronic character, including the admixtures of the charge-transfer and exciton configurations of P*. There is good evidence that the electronic composition of P* affects its internal conversion rate.[108−111] To explain the detergent-dependent P* lifetime in D_{LL}, the contributions of one or both charge-transfer configurations would be enhanced in LDAO compared to in Deriphat, especially for the shorter-lived P* subpopulation. Additional factors may distinguish the different P* forms and may vary over a distribution of values. However, the simple heterogeneous-RC model for D_{LL} at 77 K involving just two independent forms of P* is straightforward and provides a useful and consistent platform for understanding the even more complex data for D_{LL}-FY_LF_M discussed in the next section.

Heterogeneous-RC Model for D_{LL}-FY_LF_M in Deriphat Glass. In the Results section, the time-resolved absorption measurements on D_{LL}-FY_LF_M in Deriphat glass were presented in terms of a static-heterogeneity model involving two subpopulations of RCs that have very different photophysics/photochemistry (Figure 9A). The P* lifetimes in these roughly equal fractions are 35 and 410 ps based on global analysis. In the longer-lived fraction, P* deactivation to the ground state dictates the 410 ps P* lifetime. This value is essentially the same as the longer P* lifetime (430 ps) derived from the biexponential global analysis of D_{LL} in Deriphat glass (Table 1). It is not evident a priori that the longer-lived form of P* in D_{LL} and the nonphotochemically active form of P* in D_{LL}-FY_LF_M should be equated and have the same lifetime since the two RCs differ in three key amino acids that interact with P. However, the agreement between these two kinetics constants is a compelling parallel and supports the conclusion that nearly half the population of P* in D_{LL}-FY_LF_M in Deriphat glass decays by P* → ground state with a time constant of ∼400 ps.

The remaining 50% of D_{LL}-FY_LF_M is photochemically active. In this subpopulation P* has a significantly shorter lifetime (35 ps), and P* → $P^+H_M^-$ charge separation occurs with ≥80% yield. This estimate comes from several observations. First, neither the P Q_Y bleaching decay (835−865 nm) nor the P Q_X bleaching decay (590−610 nm) exhibits a 35 ps ground state recovery component. This indicates that P* internal conversion has a yield of <10% (based on the signal-to-noise), implying a yield of electron transfer to H_M of >90%. A second estimate comes from considering competing P* decay to the ground state, using the shorter, 160 ps P* lifetime for D_{LL} in Deriphat glass (Table 1). Using 35 ps for the P* lifetime in D_{LL}-FY_LF_M and 160 ps as the inherent time constant for competing P* → ground

state gives a 45 ps time constant for P* → $P^+H_M^-$ and a corresponding yield of 77%. A high yield of $P^+H_M^-$ is also consistent with the substantial amplitude of H_M bleaching at 529 nm in D_{LL}-FY_LF_M (140 ps spectrum in Figure 8), although quantitation is difficult due to the complexities of the spectral data. On the basis of these collective findings, we conclude that the $P^+H_M^-$ yield is ≥80% in the 50% subpopulation that is photochemically active.

Once $P^+H_M^-$ forms from the photoactive P* population in D_{LL}-FY_LF_M in Deriphat glass, its spectrum persists past 3.2 ns (Figures 6A and 8A), indicating that the $P^+H_M^-$ lifetime is on the order of 10 ns. This lifetime is at least a factor of 2 longer than the $P^+H_M^-$ lifetime of 3.0 ± 0.8 ns found previously from nanosecond pump−probe experiments on the YFH RC at 295 K.[81] In both cases this lifetime reflects charge recombination since electron transfer from H_M^- to Q_B is blocked by addition of terbutryn. Charge recombination may return $P^+H_M^-$ to the ground state, or lead to formation of the triplet excited state of P (^{3}P) following spin rephasing from the singlet to triplet forms of $P^+H_M^-$. For the YFH RC at 295 K, the yield of ^{3}P was found to be <5%, so the ∼3 ns lifetime of $P^+H_M^-$ reflects charge recombination to the ground state. For D_{LL}-FY_LF_M at 77 K, the somewhat longer $P^+H_M^-$ lifetime should afford a higher triplet yield (e.g., ∼10%). If so, future analysis of the temperature dependence of the ^{3}P decay could give the free energy of $P^+H_M^-$ relative to P* (^{1}P),[112] but this measurement is beyond the scope of the present study. The two potential decay pathways of $P^+H_M^-$ are analogous to the well-studied decay pathways of $P^+H_L^-$ in wild-type RCs with Q_A removed or pre-reduced. There $P^+H_L^-$ decays with a lifetime of ∼10 ns at 295 K and ∼20 ns at 77 K, although the precise lifetime as well as the fraction of charge recombination that leads to the ground state versus ^{3}P depends on conditions.[26,71,113−116] Overall our results here indicate that the temperature dependence of $P^+H_M^-$ decay is similar to that of $P^+H_L^-$ in showing a small decrease between 295 and 77 K.

A heterogeneous-RC model similar to the one developed here for D_{LL}-FY_LF_M in Deriphat glass at 77 K has been applied previously to YFH in Deriphat at 295 K.[39] The YFH mutant has two of the same changes incorporated in the D_{LL}-FY_LF_M mutant, namely, Tyr substituted at L181 ("Y_L") and Phe substituted at M208 ("F_M"). The third mutation in YFH is a His substituted at M212 that results in the incorporation of BChl (denoted β) in place of H_L; D_{LL}-FY_LF_M lacks a cofactor at this position. The time evolution of the absorption changes for YFH in Deriphat at 295 K exhibit complexities similar to those found here for D_{LL}-FY_LF_M in Deriphat glass at 77 K. The heterogeneous model for YFH includes two distinct subpopulations of RCs. In a 35% subpopulation no charge separation occurs, and P* decays to the ground state with a ∼200 ps time constant. This 200 ps time constant matches well the 180 ps (average) P* lifetime found previously for D_{LL} in Deriphat at 295 K and the shorter-lived P* component (160 ps) found here for D_{LL} in Deriphat glass at 77 K. In the remaining 65% of the YFH RCs, P* has a 30 ps lifetime and decays by charge separation to both the L and M sides, yielding a mixture of $P^+\beta^-$ and $P^+H_M^-$.

Although different charge-separated states are formed in YFH versus D_{LL}-FY_LF_M, there are clear similarities between the behavior of YFH in Deriphat at 295 K and of D_{LL}-FY_LF_M in Deriphat glass at 77 K. The similarities include the following: (1) there appear to be two populations of RCs with different photochemical behavior, (2) at the least, biexponential fits to the data are required, (3) in a significant fraction of the RCs, P* decays to the ground state with little or no competing electron transfer, (4) P* stimulated emission is observed over several hundred picoseconds, and (5) the simplest model consistent with all the spectral and kinetic data involves static heterogeneity with two distinct subpopulations of P*. YFH in Deriphat at 295 K and D_{LL}-FY_LF_M in Deriphat glass at 77 K therefore represent extreme examples of RC heterogeneity, in which subpopulations of P* are distinguished not by different rates of electron transfer, as has previously been observed for other RCs, but the capacity to perform electron transfer at all.

Homogeneous-RC Models for D_{LL} and D_{LL}-FY_LF_M at 77 K. In the prior analysis of YFH in Deriphat at 295 K,[39] additional models were considered that involve a homogeneous population of RCs. The models all involved the formation of a photochemically inactive state that does not perform electron transfer to either H_M or β but, rather, decays only to the ground state. The inactive state considered most likely was a "relaxed" form of P*, which is produced directly from the initial form of P* or indirectly from an intermediate such as $P^+B_L^-$. $P^+B_L^-$ itself was not considered a likely candidate for the inactive state because $P^+B_L^-$ would not give rise to the observed long-lived stimulated emission unless it thermally repopulated the initial form of P* or decayed by charge recombination to a "relaxed" form of P* like the one considered above.

Similar reasoning applies to homogeneous-RC models for D_{LL} and D_{LL}-FY_LF_M at 77 K. In order to be consistent with the data for both mutants the model must adhere to additional constraints that help identify the photophysical processes underlying the observed kinetics. The observation of a long-lived component of P* stimulated emission (∼400 ps) for both mutants in Deriphat glass supports the assignment of this signal to a relaxed form of P* that is incapable of electron transfer and deactivates only to the ground state (Figure 9B).

It is improbable that the decay of a charge-separated state such as $P^+B_L^-$ (formed from P*) could be directly responsible for the ∼400 ps component in either D_{LL} or D_{LL}-FY_LF_M, since this state would not give stimulated emission. Furthermore, it is improbable that, if formed, $P^+B_L^-$ would decay primarily by uphill thermal repopulation of the initial form of P* at 77 K unless the energy gap in both D_{LL} and D_{LL}-FY_LF_M RCs is less than 0.005 eV. This is a highly unlikely coincidence since the oxidation potential of P is >100 meV higher in D_{LL} than in D_{LL}-FY_LF_M. In addition, for both mutants the as-acquired and the global-analysis-derived spectra of the 400 ps component lack spectral signatures that can be readily attributed to $P^+B_L^-$. Given these constraints, a homogeneous-RC model consistent with both D_{LL} and D_{LL}-FY_LF_M RCs at 77 K most likely involves the initial P* form decaying to a relaxed P*form, either directly or via $P^+B_L^-$, that then deactivates to the ground state in ∼400 ps (Figure 9, parts B and C).

The fundamental difference between the heterogeneous- and homogeneous-RC models is whether the two principal kinetic components observed derive from (1) two initial, kinetically uncoupled forms of P* or (2) an initial and a relaxed form of P*. Fortunately, in the case of D_{LL}-FY_LF_M the same general conclusions emerge from both models: the short-lived (initial) P* form is capable of electron transfer to H_M, whereas a longer-lived P* form is not.

Temperature Dependence of M-Side Charge Separation in D_{LL}-FY_LF_M. We previously showed that for D_{LL}-FY_LF_M in Deriphat at 295 K, P* decay is well described by a single exponential (∼55 ps time constant) and gives a 70% yield of $P^+H_M^-$ and a 30% yield of deactivation to the ground state.[89] These values give a rate constant for electron transfer from P* to $P^+H_M^-$ of 0.7/(55 ps) = $(78\ \text{ps})^{-1}$. For D_{LL}-FY_LF_M in

Deriphat glass, P* in the photoactive RCs has a 35 ps lifetime and P* → $P^+H_M^-$ electron transfer occurs with high yield (≥80%) based on the heterogeneous-RC model (Figure 9A). These values give a rate constant of at least 0.80/(35 ps) = (44 ps)$^{-1}$, indicating that the P* → $P^+H_M^-$ charge separation process is roughly a factor of 2 *faster* at 77 than at 295 K. As described in the Introduction, this same roughly 2-fold increase at 77 versus 295 K is well documented for the overall L-side process P* → $P^+H_L^-$. If we also consider some simple homogeneous-RC models for D_{LL}-FY_LF_M a range of rates and yields is consistent with the data; some typical values for rate constants are detailed in Figure 9, parts B and C. On the basis of these values the rate constant for M-side electron transfer in D_{LL}-FY_LF_M at 77 K differs from that at 295 K by no more than a factor of 2. Thus, the general conclusion derived from the models explored here is that the M-side P* → $P^+H_M^-$ process in D_{LL}-FY_LF_M and the L-side P* → $P^+H_L^-$ process in wild-type RCs both have a very weak temperature dependence.

As noted in the Introduction, the same is true of the M-side process P* → $P^+\Phi_B^-$ in the H(L182)L mutant, wherein Φ_B is a bacteriopheophytin that replaces B_M and $P^+\Phi_B^-$ is below both P* and $P^+H_B^-$ in free energy.[76] This common weak temperature dependence holds for all of these processes initiated in P* despite up to 20-fold differences in rate at a given temperature and presumably different underlying predominant mechanisms (e.g., a two-step process involving $P^+B_L^-$ formation as an intermediate between P* and $P^+H_L^-$ on the L side of wild type compared to a one-step superexchange process that utilizes $P^+B_M^-$ as a virtual intermediate for the formation of $P^+H_M^-$ in D_{LL}-FY_LF_M). The comparisons can be extended to include the $P^+H_M^-$ → $P^+Q_A^-$ process in the wild-type RC, which has a rate constant of ∼(200 ps)$^{-1}$ at 295 K and ∼(100 ps)$^{-1}$ at 100 K and below.[15] Thus, the weak temperature dependence of electron transfer in the RC spans processes involving a nearly a 100-fold variation in rate constants, different degrees of electronic coupling, and different underlying mechanisms on the L and M branches.

Most descriptions of the rates of RC electron-transfer processes as a function of temperature are cast in terms of the Marcus framework with quantum corrections to incorporate vibrational modes of the cofactors and protein.[117−120] It is also typically assumes that any vibrational or structural relaxations resulting from excitation or previous charge separation steps are complete prior to the electron-transfer process of interest. If vibrational or structural relaxations are incomplete on the time scale of electron transfer, then the temperature (and free energy) dependence of a reaction's rate may be weaker than if the states are fully relaxed.[29,106,121]

Within the quantum-corrected Marcus formalism assuming equilibrated states, the reactions described above, including P* → $P^+H_M^-$, are in the so-called activationless regime in which the free energy change ($\Delta\Delta G$) is comparable to the reorganization energy (λ). A rather weak temperature dependence is also anticipated for electron transfer in the inverted region ($\Delta\Delta G > \lambda$) when quantum effects are considered. Our results rule out the possibility that the process lies in the normal activated region ($\Delta\Delta G < \lambda$) where the reaction should slow down substantially at low temperature. With the use of the values given in the Introduction and depicted in Figure 2, the free energy change for P* → $P^+H_M^-$ in the D_{LL}-FY_LF_M is estimated to be on the order of 0.1 eV. This value is comparable to the reorganization energy estimated for electron transfer from P* to the L-side cofactors in the wild-type RC.[24,25,29] Thus, the P* → $P^+H_M^-$ process in D_{LL}-FY_LF_M would appear to be in the activationless regime, or nearly so.

In the activationless regime a 2-fold increase in rate with a reduction in temperature is consistent with the temperature dependence of the thermally weighted Franck−Condon factor. Alternatively, the 2-fold rate increase could derive from the temperature dependence of the electronic factor, which may arise from the protein shrinking slightly at low temperature and thereby bringing the cofactors closer together. One or both of these two factors can account for the 2-fold increase of rate of the M-side reaction P* → $P^+H_M^-$ between 295 and 77 K.

Conclusions

We have shown that M-side electron transfer to the acceptor H_M occurs in D_{LL}-FY_LF_M RCs at 77 K. The data and analysis are complex and require models to account for the pronounced nonuniformity of the P* kinetics and the states produced by P* decay. In particular, the application of the heterogeneous-RC model leads to the conclusion that about half of D_{LL}-FY_LF_M RCs are incapable of electron transfer to H_M at 77 K. However, regardless of the model used, one remarkable conclusion is the same: M-side electron transfer P* → $P^+H_M^-$ is only weakly temperature-dependent, suggesting that, like the L-side process, the reaction is fundamentally activationless.

Acknowledgment. We thank William Childs for the up-conversion measurements. This work was supported by Grants from the National Science Foundation (MCB-0416623 to S.G.B. and MCB-0614529 to D.H. and C.K.) and a Hertz Graduate Fellowship to J.I.C.

References and Notes

(1) Deisenhofer, J.; Epp, O.; Miki, K.; Huber, R.; Michel, H. *Nature* **1985**, *318*, 618−624.
(2) Allen, J. P.; Feher, G.; Yeates, T. O.; Komiya, H.; Rees, D. C. *Proc. Natl. Acad. Sci. U.S.A.* **1987**, *84*, 5730−5734.
(3) Allen, J. P.; Feher, G.; Yeates, T. O.; Komiya, H.; Rees, D. C. *Proc. Natl. Acad. Sci. U.S.A.* **1987**, *84*, 6162−6166.
(4) Yeates, T. O.; Komiya, H.; Chirino, A.; Rees, D. C.; Allen, J. P.; Feher, G. *Proc. Natl. Acad. Sci. U.S.A.* **1988**, *85*, 7993−7997.
(5) El-Kabbani, O.; Chang, C. H.; Tiede, D. M.; Norris, J. R.; Schiffer, M. *Biochemistry* **1991**, *30*, 5361−5369.
(6) Ermler, U.; Fritsch, G.; Buchanan, S. K.; Michel, H. *Structure* **1994**, *2*, 925−936.
(7) Woodbury, N. W.; Becker, M.; Middendorf, D.; Parson, W. W. *Biochemistry* **1985**, *24*, 7516−7521.
(8) Martin, J. L.; Breton, J.; Hoff, A. J.; Migus, A.; Antonetti, A. *Proc. Natl. Acad. Sci. U.S.A.* **1986**, *83*, 957−961.
(9) Breton, J.; Martin, J. L.; Migus, A.; Antonetti, A.; Orszag, A. *Proc. Natl. Acad. Sci. U.S.A.* **1988**, *83*, 5121−5125.
(10) McDowell, L. M.; Kirmaier, C.; Holten, D. *J. Phys. Chem.* **1991**, *95*, 3379−3383.
(11) Fleming, G. R.; Martin, J. L.; Breton, J. *Nature* **1988**, *333*, 190−192.
(12) Nagarajan, V.; Parson, W. W.; Gaul, D.; Schenck, C. *Proc. Natl. Acad. Sci. U.S.A.* **1990**, *87*, 7888−7892.
(13) Lauterwasser, C.; Finkele, U.; Scheer, H.; Zinth, W. *Chem. Phys. Lett.* **1991**, *183*, 471−477.
(14) Huppman, P.; Arlt, T.; Penzkofer, H.; Schmidt, S.; Bibikova, M.; Dohse, B.; Oesterhelt, D.; Wachtveit, J.; Zinth, W. *Biophys. J.* **2002**, *82*, 3186−3197.
(15) Kirmaier, C.; Holten, D.; Parson, W. W. *Biochim. Biophys. Acta* **1985**, *810*, 33−48.
(16) Kirmaier, C.; Holten, D. *Proc. Natl. Acad. Sci. U.S.A.* **1990**, *97*, 3522−3556.
(17) Chan, C.-K.; Chen, L. X.-Q.; DiMagno, T. J.; Hanson, D. K.; Nance, S. L.; Schiffer, M.; Norris, J. R.; Fleming, G. R. *Chem. Phys. Lett.* **1991**, *176*, 366−372.
(18) Vos, M. H.; Lambry, J. C.; Robles, S. J.; Youvan, D. C.; Breton, J.; Martin, J. L. *Proc. Natl. Acad. Sci. U.S.A.* **1991**, *88*, 8885−8889.
(19) Du, M.; Rosenthal, S. J.; Xie, X.; DiMagno, T. J.; Schmidt, M.; Hanson, D. K.; Schiffer, M.; Norris, J. R.; Fleming, G. R. *Proc. Natl. Acad. Sci. U.S.A.* **1992**, *89*, 8517−8521.

(20) Taguchi, A. K.; Stocker, J. W.; Alden, R. G.; Causgrove, T. P.; Peloquin, J. M.; Boxer, S. G.; Woodbury, N. W. *Biochemistry* **1992**, *31*, 10345−10355.
(21) Small, G. J.; Hayes, J. M.; Silbey, R. J. *J. Phys. Chem.* **1992**, *96*, 7499−7501.
(22) Vos, M. H.; Lambry, J. C.; Robles, S. J.; Youvan, D. C.; Breton, J.; Martin, J. L. *Proc. Natl. Acad. Sci. U.S.A.* **1992**, *89*, 613−617.
(23) Hamm, P.; Gray, K. A.; Oesterhelt, D.; Feick, R.; Scheer, H.; Zinth, W. *Biochim. Biophys. Acta* **1993**, *1142*, 99−105.
(24) Jia, Y.; DiMagno, T. J.; Chan, C.-K.; Wang, Z.; Du, M.; Hanson, D. K.; Schiffer, M.; Norris, J. R.; Fleming, G. R.; Popov, M. S. *J. Phys. Chem.* **1993**, *97*, 13180−13191.
(25) Wang, Z. Y.; Pearlstein, R. M.; Jia, Y. W.; Fleming, G. R.; Norris, J. R. *Chem. Phys.* **1993**, *176*, 421−425.
(26) Ogrodnik, A.; Keupp, W.; Volk, M.; Aumeier, G.; Michel-Beyerle, M. E. *J. Phys. Chem.* **1994**, *98*, 3432−3439.
(27) Rautter, J.; Lendzian, F.; Lubitz, W.; Wang, S.; Allen, J. P. *Biochemistry* **1994**, *33*, 12077−12084.
(28) Wang, S.; Lin, S.; Woodbury, N. W.; Allen, J. P. *Photosynth. Res.* **1994**, *42*, 203−215.
(29) Bixon, M.; Jortner, J.; Michel-Beyerle, M. E. *Chem. Phys.* **1995**, *197*, 389−404.
(30) Stanley, R. J.; Boxer, S. G. *J. Phys. Chem.* **1995**, *99*, 859−863.
(31) Beekman, L. M. P.; van Stokkum, I. H. M.; Monshouwer, R.; Rijnders, A. J.; McGlynn, P.; Visschers, R. W.; Jones, M. R.; van Grondelle, R. *J. Phys. Chem.* **1996**, *100*, 7256−7268.
(32) Gast, P.; Hemelrijk, P. W.; VanGorkom, H. J.; Hoff, A. J. *Eur. J. Biochem.* **1996**, *239*, 805−809.
(33) Lin, S.; Xiao, W.; Eastman, J. E.; Taguchi, A. K. W.; Woodbury, N. W. *Biochemistry* **1996**, *35*, 3187−3196.
(34) Kalman, L.; Maroti, P. *Biochemistry* **1997**, *36*, 15269−15276.
(35) Laible, P. D.; Greenfield, S. R.; Wasielewski, M. R.; Hanson, D. K.; Pearlstein, R. M. *Biochemistry* **1997**, *36*, 8677−8685.
(36) Muh, F.; Rautter, J.; Lubitz, W. *Biochemistry* **1997**, *36*, 4155−4162.
(37) Lin, S.; Jackson, J.; Taguchi, A. K. W.; Woodbury, N. W. *J. Phys. Chem. B* **1998**, *102*, 4016−4022.
(38) Eastman, J. E.; Taguchi, A. K. W.; Lin, S.; Jackson, J. A.; Woodbury, N. W. *Biochemistry* **2000**, *39*, 14787−14798.
(39) Kirmaier, C.; Laible, P. D.; Hinden, E.; Hanson, D. K.; Holten, D. *Chem. Phys.* **2003**, *294*, 305−318.
(40) Baciou, L.; Sebban, P. *Photochem. Photobiol.* **1995**, *62*, 271−278.
(41) Sebban, P.; Wraight, C. A. *Biochim. Biophys. Acta* **1989**, *974*, 54−65.
(42) Gao, J.-L.; Shopes, R. J.; Wraight, C. A. *Biochim. Biophys. Acta* **1991**, *1056*, 259−272.
(43) Becker, M.; Nagarajan, V.; Middendorf, D.; Parson, W. W.; Martin, J. E.; Blankenship, R. E. *Biochim. Biophys. Acta* **1991**, *1057*, 299−312.
(44) Muh, F.; Schulz, C.; Schlodder, E.; Jones, M. R.; Rautter, J.; Kuhn, M.; Lubitz, W. *Photosynth. Res.* **1998**, *55*, 199−205.
(45) Muller, M. G.; Griebenow, K.; Holzarth, A. R. *Chem. Phys. Lett.* **1992**, *199*, 465−469.
(46) Beekman, L. M. P.; Visschers, R. W.; Monshouwer, R.; Heer-Dawson, M.; Mattioli, T. A.; McGlynn, P.; Hunter, C. N.; Robert, B.; Van Stokkum, I. H. M.; Van Grondelle, R.; Jones, M. R. *Biochemistry* **1995**, *34*, 14712−14721.
(47) Haffa, A. L. M.; Lin, S.; Williams, J. C.; Bowen, B. P.; Taguchi, A. K. W.; Allen, J. P.; Woodbury, N. W. *J. Phys. Chem. B* **2004**, *108*, 4−7.
(48) Tiede, D. M.; Kellogg, E. C.; Breton, J. *Biochim. Biophys. Acta* **1987**, *892*, 294−302.
(49) Parot, P.; Thiery, J.; Vermeglio, A. *Biochim. Biophys. Acta* **1987**, *893*, 534−543.
(50) Parson, W. W.; Chu, Z. T.; Warshel, A. *Biochim. Biophys. Acta* **1990**, *1017*, 251−272.
(51) Alden, R. G.; Parson, W. W.; Chu, Z. T.; Warshel, A. *J. Phys. Chem.* **1996**, *100*, 16761−16770.
(52) Gunner, M. R.; Nicholls, A.; Honig, B. *J. Phys. Chem.* **1996**, *100*, 4277−4291.
(53) Thompson, M. A.; Zerner, M. *J. Am. Chem. Soc.* **1991**, *113*, 8210−8215.
(54) Blomberg, M. R. A.; Siegbahn, P. E. M.; Babcock, G. T. *J. Am. Chem. Soc.* **1998**, *120*, 8812−8824.
(55) Steffen, M. A.; Lao, K.; Boxer, S. G. *Science* **1994**, *264*, 810−816.
(56) Palaniappan, V.; Bocian, D. *J. Am. Chem. Soc.* **1995**, *117*, 3647−3648.
(57) van Dijk, B.; Hoff, A. J.; Shkuropatov, A. Y. *J. Phys. Chem. B* **1998**, *102*, 8091−8099.
(58) Fajer, J.; Borg, D. C.; Forman, A.; Dolphin, D.; Felton, R. H. *J. Am. Chem. Soc.* **1973**, *95*, 2739−2741.
(59) Fajer, J.; Brune, D. C.; Davis, M. S.; Forman, A.; Spaulding, L. D. *Proc. Natl. Acad. Sci. U.S.A.* **1975**, *72*, 4956−4960.
(60) Cotton, T. M.; Van Duyne, R. P. *J. Am. Chem. Soc.* **1979**, *101*, 7605−7612.
(61) Felton, R. H. Primary Redox Reactions of Metalloporphyrins. In *The Porphyrins*; Dolphin, D. Ed.; Academic Press: New York, 1978; Vol. V, pp 53−125.
(62) Schmidt, S.; Arlt, T.; Hamm, P.; Huber, H.; Nagele, T.; Wachtveitl, J.; Zinth, W.; Meyer, M.; Scheer, H. *Spectrochim. Acta, Part A* **1995**, *51*, 1565−1578.
(63) Schmidt, S.; Arlt, T.; Hamm, P.; Huber, H.; Nagele, T.; Wachtveitl, J.; Meyer, H.; Scheer, H.; Zinth, W. *Chem. Phys. Lett.* **1994**, *223*, 116−120.
(64) Arlt, T.; Schmidt, S.; Kaiser, W.; Lauterwasser, C.; Meyer, M.; Scheer, H.; Zinth, W. *Proc. Natl. Acad. Sci. U.S.A.* **1993**, *90*, 11757−11761.
(65) Holzwarth, A. R.; Muller, M. G. *Biochemistry* **1996**, *35*, 11802−11831.
(66) Shuvalov, V. A.; Yakovlev, A. G. *Biol. Membr.* **1998**, *15*, 455−460.
(67) Katilius, E.; Babendure, J. L.; Lin, S.; Woodbury, N. W. *Photosynth. Res.* **2004**, *81*, 165−180.
(68) Roberts, J. A.; Holten, D.; Kirmaier, C. *J. Phys. Chem. B* **2001**, *105*, 5575−5584.
(69) Kirmaier, C.; Gaul, D.; DeBey, R.; Holten, D.; Schenck, C. C. *Science* **1991**, *251*, 922−927.
(70) Heller, B. A.; Holten, D.; Kirmaier, C. *Science* **1995**, *269*, 940−945.
(71) Volk, M.; Aumeier, G.; Langenbacher, T.; Feick, R.; Ogrodnik, A.; Michel-Beyerle, M. E. *J. Phys. Chem. B* **1998**, *102*, 735−751.
(72) Gunner, M. *Curr. Top. Bioenerg.* **1991**, *16*, 319−367.
(73) Goldstein, R. A.; Boxer, S. G. *Biochim. Biophys. Acta* **1989**, *977*, 78−86.
(74) Peloquin, J. M.; Williams, J. C.; Lin, X.; Alden, R. G.; Taguchi, A. K. W.; Allen, J. P.; Woodbury, N. W. *Biochemistry* **1994**, *33*, 8089−8100.
(75) Hartwich, G.; Lossau, H.; Michel-Beyerle, M. E.; Ogrodnik, A. *J. Phys. Chem. B* **1998**, *102*, 3815−3820.
(76) Katilius, E.; Katiliene, Z.; Lin, S.; Taguchi, A. K. W.; Woodbury, N. W. *J. Phys. Chem. B* **2002**, *106*, 1471−1475.
(77) Katilius, E.; Katiliene, Z.; Lin, S.; Taguchi, A. K. W.; Woodbury, N. W. *J. Phys. Chem. B* **2002**, *106*, 12344−12350.
(78) Katilius, E.; Babendure, J. L.; Katiliene, Z.; Lin, S.; Taguchi, A. K.; Woodbury, N. W. *J. Phys. Chem. B* **2003**, *107*, 12029−12034.
(79) Kirmaier, C.; He, C.; Holten, D. *Biochemistry* **2001**, *40*, 12132−12139.
(80) Wakeham, M. C.; Jones, M. R. *Biochem. Soc. Trans.* **2005**, *133*, 851−857.
(81) Kee, H. L.; Laible, P. D.; Bautista, J. A.; Hanson, D. K.; Holten, D.; Kirmaier, C. *Biochemistry* **2006**, *45*, 7314−7322.
(82) de Boer, A. L.; Neerken, S.; de Wijn, R.; Permentier, H. P.; Gast, P.; Vijgenboom, E.; Hoff, A. J. *Biochemistry* **2002**, *41*, 3081−3088.
(83) de Boer, A. L.; Neerken, S.; de Wijn, R.; Permentier, H. P.; Gast, P.; Vijgenboom, E.; Hoff, A. J. *Photosynth. Res.* **2002**, *71*, 221−239.
(84) Paddock, M. L.; Chang, C.; Xu, Q.; Abresch, E. C.; Axelrod, H. L.; Feher, G.; Okamura, M. Y. *Biochemistry* **2005**, *44*, 6920−6928.
(85) Paddock, M. L.; Flores, M.; Isaacson, R.; Chang, C.; Abresch, E. C.; Selvaduray, P.; Okamura, M. Y. *Biochemistry* **2006**, *45*, 14032−14042.
(86) Czarnecki, K.; Kirmaier, C.; Holten, D.; Bocian, D. F. *J. Phys. Chem. A* **1999**, *103*, 2235−2246.
(87) Marchanka, A.; Paddock, M.; Lubitz, W.; van Gastel, M. *Biochemistry* **2007**, *46*, 14782−14794.
(88) Pudlak, M. *J. Chem. Phys.* **2003**, *118*, 1876−1882.
(89) Chuang, J. I.; Boxer, S. G.; Holten, D.; Kirmaier, C. *Biochemistry* **2006**, *45*, 3845−3851.
(90) Breton, J.; Martin, J. L.; Lambry, J. C.; Robles, S. J.; Youvan, D. C. Ground State and Femtosecond Transient Absorption Spectroscopy of a Mutant of *Rhodobacter capsulatus* which Lacks the Initial Electron Acceptor Bacteriopheophyrin. In *Structure and Function of Bacterial Photosynthetic Reaction Centers*; Michel-Beyerle, M. E., Ed.; Springer-Verlag: New York, 1990; pp 293−302.
(91) Robles, S. J.; Breton, J.; Youvan, D. C. *Science* **1990**, *248*, 1402−1405.
(92) Watson, A. J.; Fyfe, P. K.; Frolov, D.; Wakeham, M. C.; Nabedryk, E.; Van Grondelle, R.; Breton, J.; Jones, M. R. *Biochim. Biophys. Acta* **2005**, *1710*, 34−46.
(93) Fyfe, P. K.; Potter, J. A.; Cheng, J.; Williams, C. M.; Watson, A. J.; Jones, M. R. *Biochemistry* **2007**, *46*, 10461−10472.
(94) Stanley, R. J.; King, B.; Boxer, S. G. *J. Phys. Chem.* **1996**, *100*, 12052−12059.
(95) Kirmaier, C.; Holten, D. *Biochemistry* **1991**, *30*, 609−613.
(96) Parson, W. W.; Warshel, A. *J. Am. Chem. Soc.* **1987**, *109*, 6152−6163.
(97) Eberl, U.; Gilbert, M.; Keupp, W.; Langenbacher, T.; Siegl, J.; Sinning, I.; Ogrodnik, A.; Robles, S. J.; Breton, J.; Youvan, D. C.; Michel-Beyerle, M. E. Fast Internal Conversion in Bacteriochlorophyll Dimers. In

The Photosynthetic Reaction Center II; Vermeglio, A., Breton, J., Eds.; 1992; pp 253−260.
(98) Bylina, E. J.; Kirmaier, C.; McDowell, L. M.; Holten, D.; Youvan, D. C. *Nature* **1988**, *336*, 182−184.
(99) Kirmaier, C.; Laporte, L.; Schenck, C. C.; Holten, D. *J. Phys. Chem.* **1995**, *99*, 8903−8909.
(100) Kirmaier, C.; Cua, A.; He, C.; Holten, D.; Bocian, D. F. *J. Phys. Chem. B* **2002**, *106*, 495−503.
(101) Muh, F.; Williams, J. C.; Allen, J. P.; Lubitz, W. *Biochemistry* **1998**, *37*, 13066−13074.
(102) Peloquin, J. M.; Lin, S.; Taguchi, A. K. W.; Woodbury, N. W. *J. Phys. Chem.* **1995**, *99*, 1349−1356.
(103) Peloquin, J. M.; Lin, S.; Taguchi, A. K. W.; Woodbury, N. W. *J. Phys. Chem.* **1996**, *100*, 1428−14235.
(104) Lin, S.; Taguchi, A. K. W.; Woodbury, N. W. *J. Phys. Chem.* **1996**, *42*, 17067−17078.
(105) Woodbury, N. W.; Peloquin, J. M.; Alden, R. G.; Lin, X.; Lin, S.; Taguchi, A. K. W.; Williams, J. C.; Allen, J. P. *Biochemistry* **1994**, *33*, 8101−8112.
(106) Wang, H. Y.; Lin, S.; Allen, J. P.; Williams, J. C.; Blankert, S.; Laser, C.; Woodbury, N. W. *Science* **2007**, *316*, 747−750.
(107) Gehlen, J. N.; Marchi, M.; Chandler, D. *Science* **1994**, *263*, 499−502.
(108) Kirmaier, C.; Bylina, E. J.; Youvan, D. C.; Holten, D. *Chem. Phys. Lett.* **1989**, *159*, 251−257.
(109) McDowell, L. M.; Kirmaier, C.; Holten, D. *Biochim. Biophys. Acta* **1990**, *1020*, 239−246.
(110) McDowell, L. M.; Gaul, D.; Kirmaier, C.; Holten, D.; Schenck, C. C. *Biochemistry* **1991**, *30*, 8315−8322.
(111) Laporte, L. L.; Palaniappan, V.; Davis, D. G.; Kirmaier, C.; Schenck, C. C.; Holten, D.; Bocian, D. F. *J. Phys. Chem.* **1996**, *100*, 17696−17707.
(112) de Winter, A.; Boxer, S. G. *J. Phys. Chem. A* **2003**, *107*, 3341−3350.
(113) Parson, W. W.; Clayton, R. K.; Cogdell, R. J. *Biochim. Biophys. Acta* **1975**, *387*, 265−278.
(114) Chidsey, C. E. D.; Kirmaier, C.; Holten, D.; Boxer, S. G. *Biochim. Biophys. Acta* **1984**, *766*, 424−437.
(115) Woodbury, N. W.; Parson, W. W. *Biochim. Biophys. Acta* **1984**, *767*, 345−361.
(116) Tang, C.-K.; Williams, J. C.; Taguchi, A. K. W.; Allen, J. P.; Woodbury, N. W. *Biochemistry* **1999**, *38*, 8794−8799.
(117) Jortner, J. *J. Am. Chem. Soc.* **1980**, *102*, 6676−6686.
(118) Sari, A. *Biochim. Biophys. Acta* **1980**, *589*, 71−83.
(119) Kakitani, T.; Kakitani, H. *Biochim. Biophys. Acta* **1981**, *635*, 498−514.
(120) Marcus, R. A.; Sutin, N. *Biochim. Biophys. Acta* **1985**, *811*, 295−322.
(121) Parson, W. W.; Warshel, A. *J. Phys. Chem. B* **2004**, *108*, 10474−10483.